Korean J. Chem. Eng., 33(4), 1369-1379 (2016)
DOI: 10.1007/s11814-015-0243-3

pISSN: 0256-1115
eISSN: 1975-7220

Characterization of high-alumina coal fly ash based silicate material and its adsorption performance to CO_2

Yinan Yan, Yajun Gao, Wenjing Tang, Qiang Li, and Jianbin Zhang†

College of Chemical Engineering, Inner Mongolia University of Technology, Huhhot 010051, China
(*Received 15 June 2015 • accepted 17 November 2015*)

Abstrct–Silicate material prepared from high-alumina coal fly ash (HACFA) was characterized by using XRD, SEM, FTIR spectroscopy, TGA-DSC, and elemental analysis. These spectral results show that the silicate material is mainly composed of eight elements--O, C, Si, Ca, Na, Mg, Al, and Fe, which exist as the formations of Ca^{2+}, Na^{+}, Mg^{2+}, Al^{3+}, Fe^{3+}, SiO_3^{2-}, and CO_3^{2-}, and some adsorbed water and crystal water are determined in the silicate material. The material with surface area of 117.12 m^2/g shows a faveolate structure, and a pore size distribution of silicate material is calculated at 11.01 nm from the nitrogen desorption isotherm using the BJH model. When the material was used for CO_2 adsorption at T=323.15 K and flow rate=95 mL/min with 15.79% (vol) CO_2, a dynamic adsorption capacity of CO_2 on the surface of silicate material was found at 8.67 mg/g and the adsorption values decreased weakly after seventeen recycling times. The investigation of dynamic adsorption behavior shows that the silicate material presents similar adsorption properties with commercial active carbon and stronger adsorption properties than commercial diatomite.

Keywords: Silicate Material, High-alumina Coal Fly Ash (HACFA), Carbon Dioxide (CO_2), Adsorption, Regeneration

INTRODUCTION

Since CO_2 started being monitored in 1958, the increasing CO_2 concentration in the atmosphere has accelerated from less than 1 ppm per year prior to 1970 to more than 2 ppm per year in recent years [1]. As a result, the atmospheric level of CO_2 increased from 315 ppm in 1958 to 385 ppm in 2009 [1]. The ever increasing concentration of CO_2 in the atmosphere is requiring mankind to consider ways of controlling emissions of this greenhouse gas to the atmosphere. The phenomenon is expected to cause serious environmental hazards, which have raised the precondition for proficient capture, storage, and sequestration methodologies of CO_2 [2]. Fossil-fuel power plants are mainly responsible for CO_2 emissions [3, 4]. Hence, it is important to capture CO_2 from flue gas.

The most common processes of CO_2 separation include absorption, adsorption, gas separation membranes, and cryogenic distillation [5-8]. Absorption process, in which amine solvents are uppermost, is an important method for capturing CO_2 from various gases, including flue gas and natural gas in regenerative absorption-desorption processes. However, absorption processes have some drawbacks [9] as follows: (1) the applied solvent has limited cyclic CO_2 loading capacity; (2) it promotes corrosion of the equipment; (3) solvent regeneration requires high energy consumption; (4) a significant amount of solvent is lost by evaporation; and (5) the solvent degrades in an oxygen-rich atmosphere. Gas permeation processes have higher separation energy efficiency relative to equilibrium-based processes and high packing density which requires small installations [10]. However, for the membrane separation processes, the treatment of an enormous flow rate of flue gas emitted by power plants requires a very large membrane area and a very large, expensive, and energy-consuming compression equipment, thereby increasing the cost of this capture technology [2]. Cryogenic distillation can capture CO_2 with high purity in a liquid form, being easier to transport and store or send for enhanced oil recovery fields [11,12]; however, the energy cost is huge.

Adsorption is used as a method to eliminate CO_2 on account of higher cycle efficiency and is environmentally friendly. With the aim of increasing the efficiency of CO_2 removal processes, alternative adsorbents such as active carbon, zeolite and molecular sieves have attracted considerable attention to control CO_2 [13-15]. Physical adsorption on active carbon is widely used for the separation and purification of gases. Active carbon does not require any moisture removal and presents a high CO_2 adsorption capacity at ambient pressure; moreover, they are easy to regenerate [16]. Nevertheless, though research on active carbon production is widely performed, one-step activation method of the precursor under CO_2 flow is rarely cited [17]. Zeolite has shown promising results for separating CO_2 from gas mixtures. However, the presence of water inhibits the CO_2 adsorption capacity of zeolites [18,19]. Molecular sieves are specially designed sieves that separate molecules based on their molecular mass or molecular size. The technology is cost-effective and can be adapted to a variety of carbon sequestration schemes [20]. Unfortunately, molecular sieves often suffer from pore blocking hygroscopicity and a lack of regenerative ability.

HACFA is the incombustible residue that remains after the burning of coal in coal-fired power stations. Recycling HACFA can be a good alternative to disposal and could achieve significant economic and environmental benefits as well [21]. More aggressive efforts have been undertaken recently, to recycle fly ash [22]. For example, about 20% of the fly ash generated is used in concrete

†To whom correspondence should be addressed.
E-mail: tadzhang@pku.edu.cn
Copyright by The Korean Institute of Chemical Engineers.

Table 1. Chemical composition of coal gangue measured by XRF spectrum

Al_2O_3	SiO_2	Fe_2O_3	MgO	CaO	Na_2O	K_2O	TiO_2	MnO_2	P_2O_5	SO_3	Total
48.73	41.23	1.18	0.43	1.87	0.15	0.52	1.62	0.013	0.18	0.15	96.16

production. Other uses include soil amelioration [23,24], ceramic industry uses [25-27], catalysis and support for catalysis [28-30], adsorbents for removal of various pollutants [31,32] depth separation [33], zeolite synthesis [34-36], and valuable metals recovery [37-39]. However, there has been no report on preparation of the silicate material from HACFA.

The success of CO_2 capture using adsorption is greatly dependent on the development of a low cost and regenerable adsorbent with high CO_2 adsorption capacity [40]. In the present work, a faveolate silicate material, which comes from HACFA, is expected to be a high-performance adsorbent for CO_2 separation. Our objective was to investigate the physicochemical properties and adsorption performance of CO_2 on the surface of HACFA based silicate material. The adsorption dynamic behavior of CO_2 on the material was investigated by using an adsorption-desorption apparatus with gas chromatograph (GC) detector. The adsorption comparison of material to commercial active carbon and diatomite was obtained.

EXPERIMENTAL SECTION

1. Materials

The silicate material, which is about 0.32 dollar per 1 kg, was prepared by published methods [41,42]. The HACFA was graciously supplied by Second thermal power plant in Baotou from Inner Mongolia province and characterized by XRF analysis, as shown in Table 1. Fig. 1 shows the brief process to prepare silicate material. First, alkaline solution was blended with HACFA to get the mixture. Then to obtain silicate material, the solid part was dried after separating the mixture. Commercially produced CO_2 (purity >99.99%), N_2 (purity >99.99%), commercial active carbon (4.19 dollars per 1 kg), and commercial diatomite (about 2.42 dollars per 1 kg) were used. The surface area and pore characteristic data of commercial active carbon and diatomite are presented in Table 2.

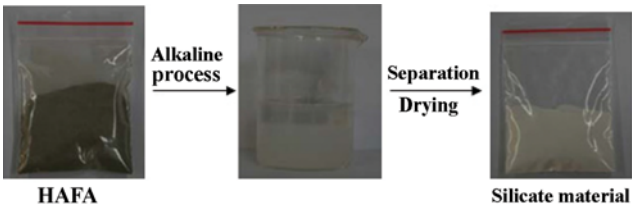

Fig. 1. Preparation process of silicate material.

Table 2. Surface area and pore characteristic data for commercial active carbon and diatomite

Material	S (m^2/g)	V (mL/g)	d (nm)
Diatomite	5.32	0.01	4.43
Active carbon	521.15	0.86	10.70

*Obtained by 3H-2000PS1/2 specific surface & pore size analysis instrument

2. Characterization

The silicate materials were characterized by using XRD analyses (Shimadzu, D/max-2200/PC) to access the structural integrity. The radiation of Cu Kα was generated using an X-ray generator. FTIR spectra of the silicate materials were recorded using KBr pellet technique (Nicolet, Nexus 670). The samples were analyzed in the wave length region of (4,000 to 400) cm^{-1}. This was done to confirm the formation of new groups, which are formed as the adsorption product of CO_2. SEM analysis was carried out using a HITACHI, S-3400N as well as the elemental analysis. TEM analysis involved a JEM-2100F. The standard BET method was used to measure the specific surface area of the adsorbent based on the physical adsorption of N_2 on the solid surface (Beishide, 3H-2000PS1/2 Specific surface & pore size analysis instrument). CO_2 adsorption-desorption isotherms were obtained by the specific surface and pore size analysis instrument. The thermal analysis of adsorbent was performed using thermogravimetry analyzer and differential scanning calorimeter (TGA-DSC) on a NETZSCH instrument. To check thermal stability, the adsorbents were heated at a rate of 10 K/min from 303.15 to 1273.15 K under N_2 with a flow rate of 20 mL/min (STP).

3. Adsorption-desorption Curves

The removal of CO_2 by the silicate material was investigated by studying the adsorption-desorption curves. In the method, the fixed column was packed with the silicate material to measure the adsorption dynamic data in the adsorption-desorption processes of CO_2.

The dynamic experimental setup in Fig. 2 was composed of gas section, reactor section, and detection section. TCD response was calibrated employing CO_2/N_2 mixtures with known composition. The three-port valves were on the positions of adsorption in the adsorptive step. The CO_2 composition in the effluent gas was continuously monitored at an interval of 3 min. As a function of time, breakthrough curve was reached until the composition approached the inlet gas composition value, that is, until saturation was reached, and then, the CO_2 flow was stopped but the N_2 flow was constant. The column was then heated to 423.15 K. At the same time, the three-port values were switched on the positions of desorption. So the methods of heating and reflux purging using N_2 were synchronized in the desorption step, which was used in cleaning the adsorbent surface. The desorption step was finished when the CO_2 composition in the effluent gas was around 0.1%.

In Fig. 2, the gas manifold system consisted of two lines which were used to feed in CO_2 and N_2. The two lines fitted with mass flow meters supply flows ranging from 1 to 500 mL/min (CO_2), and 1 to 2,000 mL/min (N_2). The controllers had an accuracy of 1.5% full scale.

A K-type thermocouple with an accuracy of 0.1 K, located at insulating layer of the adsorption column, was used to set the col-

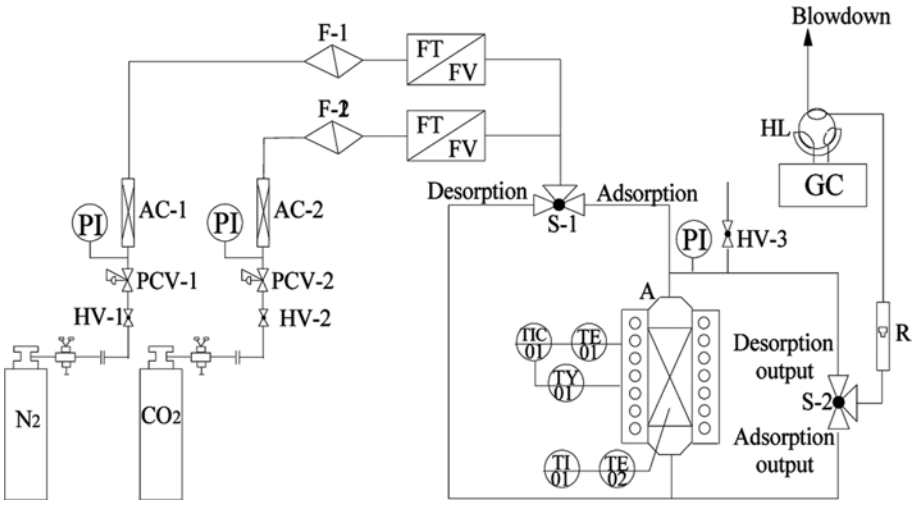

Fig. 2. Dynamic experimental setup used for adsorption-desorption studies.

HV. Stop valve	F. Filter	TE. Thermocouple	HL. Six-way valve
PCV. Counterbalance value	FT/FV. Mass flowmeter	TIC. Temperature controller	R. Rotameter
PI. Manometer	S. Three-port value	TY. Heating element	
AC. Drying tube	A. Adsorber	TI. Thermodetector	

umn temperature needed. The other K-type thermocouple continuously monitored the actual column temperature. The temperature was controlled by coupling the heating element inside of insulating layer.

The system was also equipped with a continuous gas chromatograph (TECHCOMP 7700 GC), to detect the amounts of CO_2 adsorbed from CO_2/N_2 mixtures on silicate material. GC was fitted with a carbon molecular sieve (3 mm×2,000 mm) column and a TCD detector, in which H_2 was used as the carrier gas. The outlet gases were fed to manual sampler on the GC. The GC column used was on the analysis conditions as follows: carrier gas is H_2 at 20 mL/min, temperatures are 353.15 K (oven), 373.15 K (injector), and 373.15 K (detector).

Each sample was subjected to pretreatment for the cleaning of adsorbent surface by heating on 393.15 K for 3 h. The quantity of adsorbents were kept at 130 g, and packed in a steel adsorber with an effective working length of 440 mm and an internal diameter of 40 mm. The ratio of CO_2 in the mixture CO_2/N_2 gas was fixed at 15.79%.

4. Equation of Dynamic Adsorption Capacity

The equation of dynamic adsorption capacity is

$$Q = \frac{VM_{CO_2}}{km}\int_0^t (C_0 - C_t)dt \quad (1)$$

where Q means dynamic adsorption capacity, mg/g; V is the total flow rate, mL/min; M_{CO_2} is the molar mass of CO_2, 44 g/mol; k is 22.4 L/mol; m is mass of adsorbent, 130 g; t is adsorption time, min; Co and Ct are the concentrations of CO_2 at inlet and outlet, %.

RESULTS AND DISCUSSION

1. Characterizations of Silicate Material

1-1. XRD

The XRD spectrum of original silicate material was recorded and shown in Fig. 3. A remarkable single reflection peak at 29.14°, which may correspond to calcite [43], riversideite [44], or scawtite [45], was observed. XRD result suggested the amorphous, unordered morphology, and impure adsorbent formation (Fig. 3).

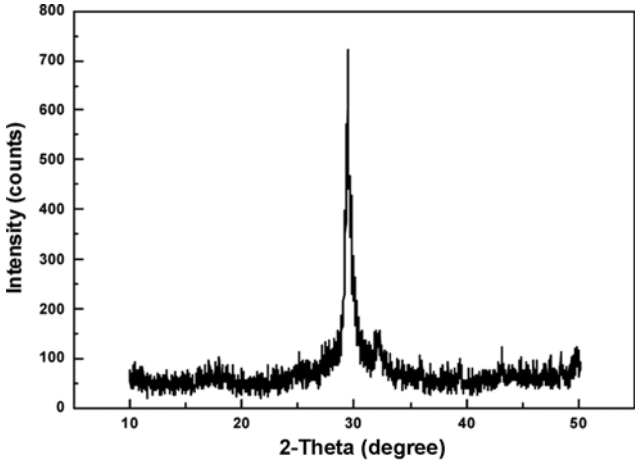

Fig. 3. XRD spectrum of silicate material.

1-2. SEM

A distinct surface morphology of silicate material was observed through SEM images (Fig. 4). Their particle morphology is useful for understanding the physical properties of material. The microstructure of material affects the binding and sorption properties. From Fig. 4, the silicate material consists of particles with irregular shape and size. A significant fraction of particles have a rough surface; others form unevenly shaped aggregates. The particles of silicate material show (40-50) μm (Fig. 4(a)), and the silicate material has lamina structure with thickness of about 30 nm and faveolate structure with (3-5) μm (Fig. 4(b)). The material has probably provided a rough surface for CO_2 adsorption, as suggested in BET

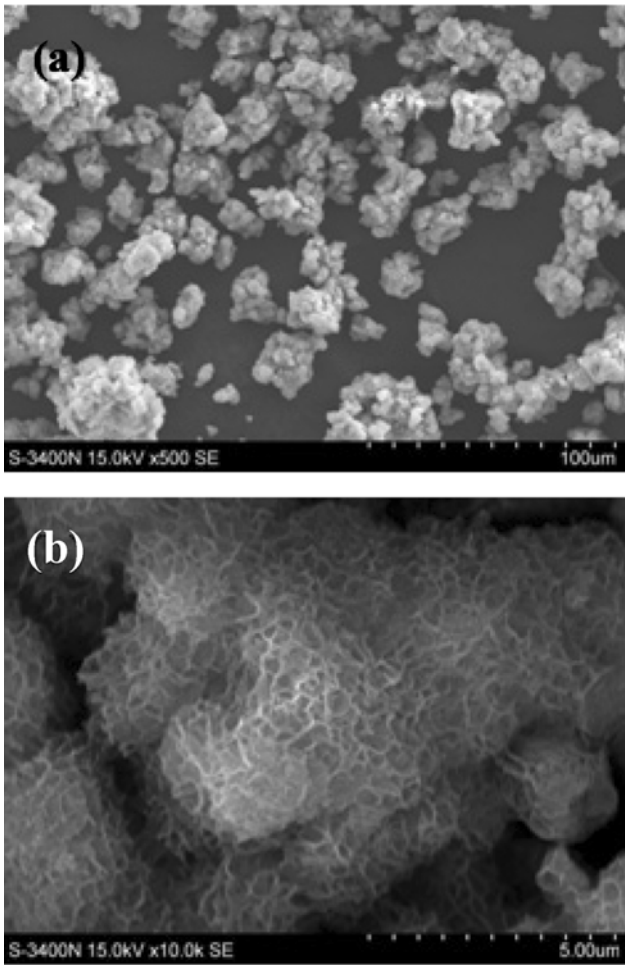

Fig. 4. SEM images of silicate material of (a) ×500 and (b) ×10.0 k.

results.

The elements of silicate material are detected by using the energy spectrum configured in the SEM. The elemental analysis data provided significant information about elemental content of silicate material as follows (Fig. 5 and Table 3).

From Table 4 and Fig. 5, the silicate material is mainly composed of eight elements: O, C, Si, Ca, Na, Mg, Al, and Fe. The content of oxygen element is 60.09%, the content of carbon element is 20.67%, and content of silicon element is 9.33%. Based on the energy spectrum and the following FTIR spectrum, SiO_3^{2-} and CO_3^{2-} can be speculated in the adsorbent.

1-3. TEM

Fig. 6(a) and (b) show the TEM images of silicate material interfaces.

From Fig. 6(a) and (b), the silicate material surface appears homogeneously covered with about 5 to 10 nm range skeleton structure.

1-4. FTIR

In Fig. 7, the FTIR spectrum represents a strong and broad band

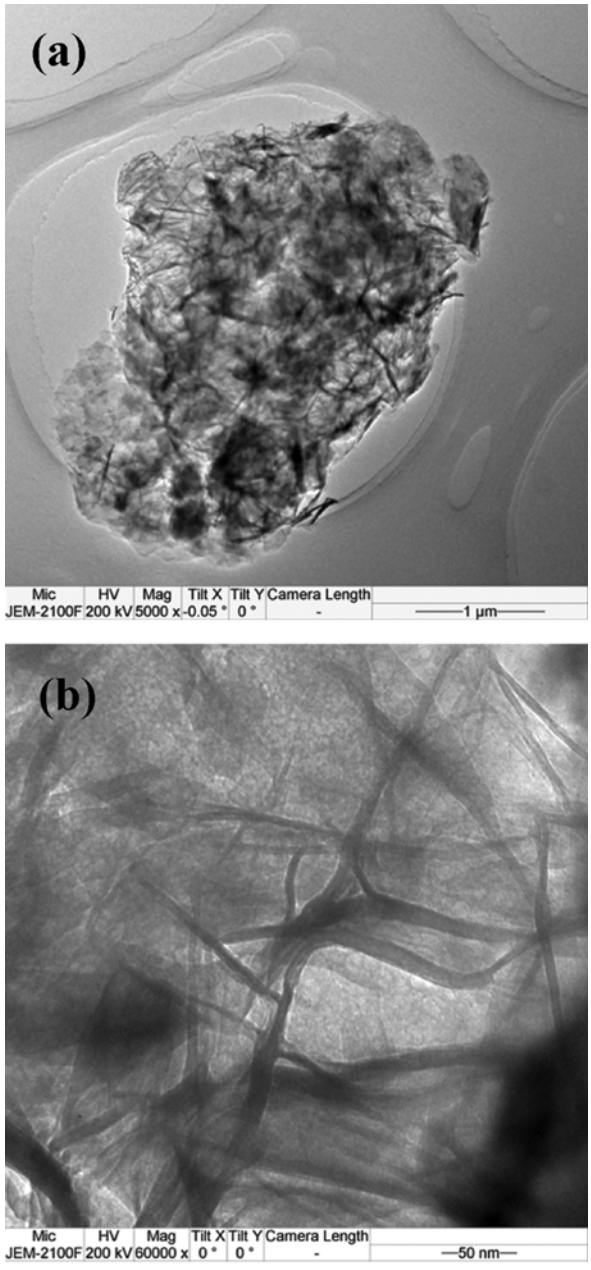

Fig. 5. TEM images of silicate material of (a) ×5.0 and (b) ×60.0 k.

Table 3. Elemental analysis of silicate material

Element	C	O	Na	Mg	Al	Si	Ca	Fe
Weight%	13.68	52.98	3.4	0.52	0.34	14.44	14.44	0.2
Atomic%	20.67	60.09	2.69	0.39	0.23	9.33	6.54	0.06

at 3,475 cm^{-1}, which was attributed to the multi-molecular association O-H stretching vibration in -Si-O-H and trapped molecular

Table 4. Surface area and pore characteristic data of silicate material

Material	S_{BJH} (m^2/g)	S-$M_{t\text{-}plot}$ (m^2/g)	S-$E_{t\text{-}plot}$ (m^2/g)	V_{BJH} (mL/g)	V-$E_{t\text{-}plot}$ (mL/g)	d (nm)
Silicate material	117.12	14.23	102.88	0.36	0.0065	11.01

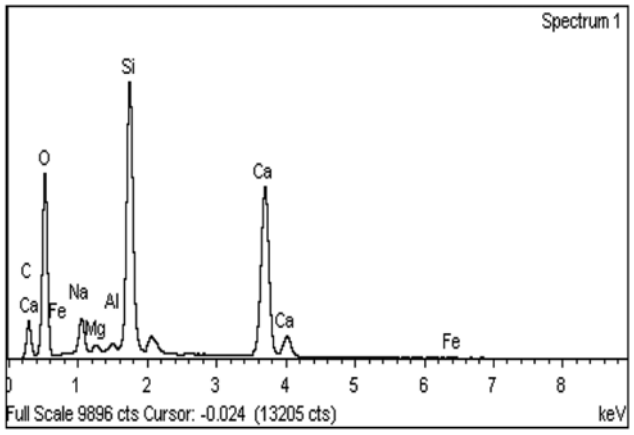

Fig. 6. Energy spectrum of silicate material.

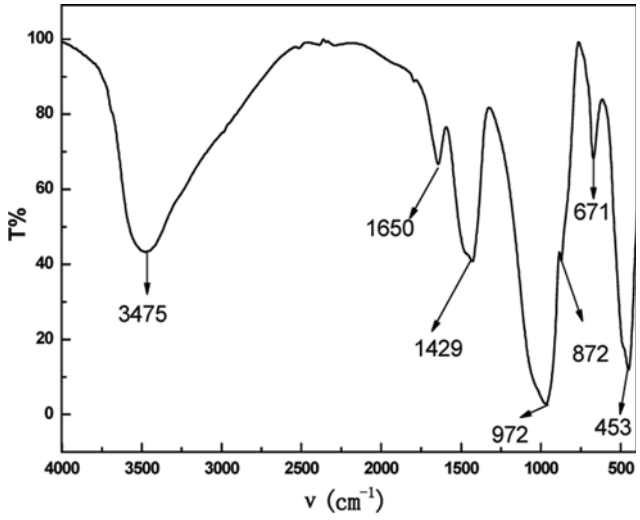

Fig. 7. FTIR spectrum of silicate material.

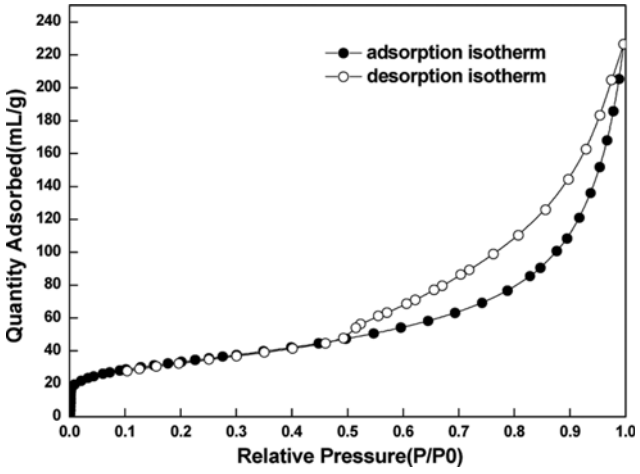

Fig. 8. Nitrogen adsorption-desorption isotherms of silicate material.

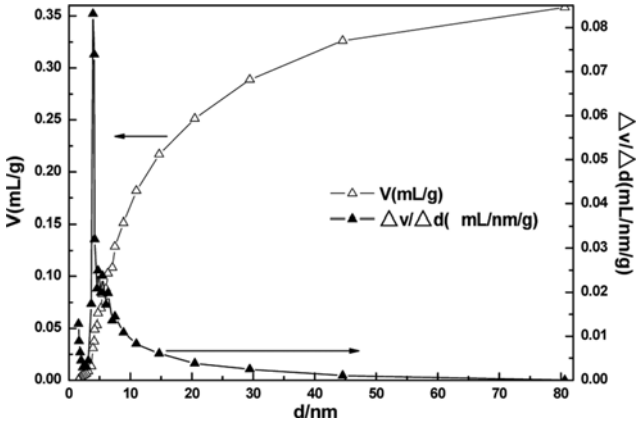

Fig. 9. Pore size distribution curve of silicate material.

water [46]. The presence of weak peak at 1,650 cm^{-1} can be attributed to H-O-H bending vibration of molecular water that is weakly physisorbed on the surface [47]. Fig. 6 shows that there is adsorbed water and/or crystal water in the silicate material. The peak at 671 cm^{-1} is due to stretching vibration of C-O, and the strong peak at 1,429 cm^{-1} and the weak peak at 872 cm^{-1} are due to the existence of $CaCO_3$ [48]. The strong peak at 972 cm^{-1} means the existence of the stretching vibration band of terminal Si-OH on the silicate surface [49]. And the peak at 453 cm^{-1} is due to the silica network with Si-O-Si vibration [44]. The FTIR results clearly confirm that the silicate material contains Si-OH, SiO_3^{2-}, $CaCO_3$, some adsorbed water, and/or crystal water.

1-5. BET Surface Area and Pore Analysis

The nitrogen adsorption-desorption isotherms of silicate material are shown in Fig. 8 and Table 3. Table 3 shows the specific surface area of silicate material is 117.12 m^2/g, which is calculated by using BET method. Note that the initial part of the adsorption isotherms at lower relative pressure (P/P_0) below 0.07, where the nitrogen uptake increases sharply with the increment of relative pressure, proves a little portion of existence of micropore structure. However, for the silicate material, the slope of the plateau at medium relative pressures and accelerated uptakes at higher relative pressure are the evidence of capillary condensation of nitrogen within the primary mesopore. According to IUPAC classification, the silicate material is typical of adsorbent with a predominantly mesoporous structure, as the majority of pore-filling occurs at relative pressures from (0.5 to 1). The pore size distribution of the adsorbent calculated by applying the BJH (Barrett-Joyner-Halenda) theory to the N_2 adsorption-desorption isotherms at 77 K is shown in Fig. 9. It is clearly shown that silicate material is a mesopore adsorbent with a unimodal pore distribution between 3 nm and 20 nm, additionally. Fig. 9 shows another small pore system with micropore (1.5-2.0) nm. The adsorption studies indicate the material shows defined mesopore, thick, and dense wall structure. On the other hand, the average pore diameter 11.01 nm and specific pore volume 0.36 mL/g of silicate material show the possible adsorption sites for various gases. In Table 3, the micropore surface areas of silicate material is 14.23 m^2/g, the external surface areas is 102.88 m^2/g, and the micropore volume is 0.0065 mL/g by using t-plot method.

1-6. TGA-DSC

The thermal stability of silicate material was observed by TGA-DSC analysis, as shown in Fig. 10. From Fig. 10, the silicate mate-

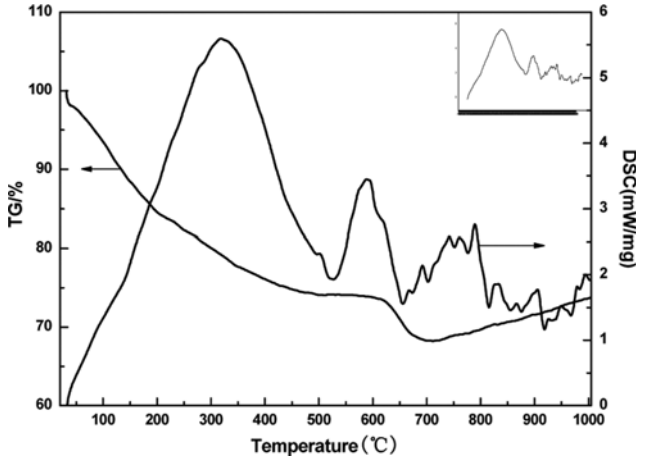

Fig. 10. TGA-DTA of silicate material.

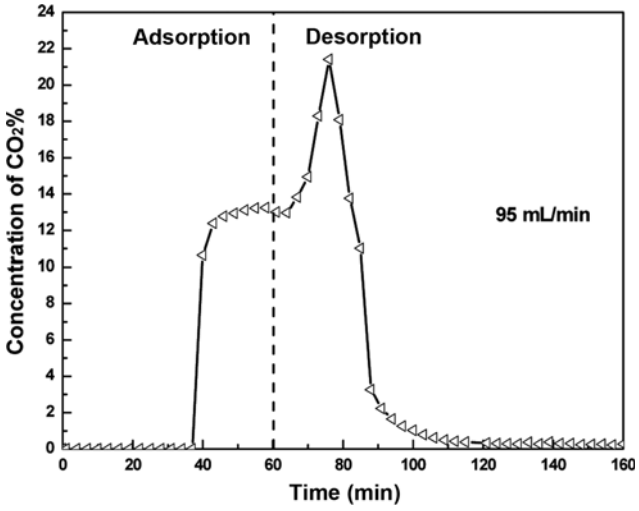

Fig. 11. Adsorption-desorption curves at flow rate of is 95 mL/min and adsorption temperature is at 303.15 K.

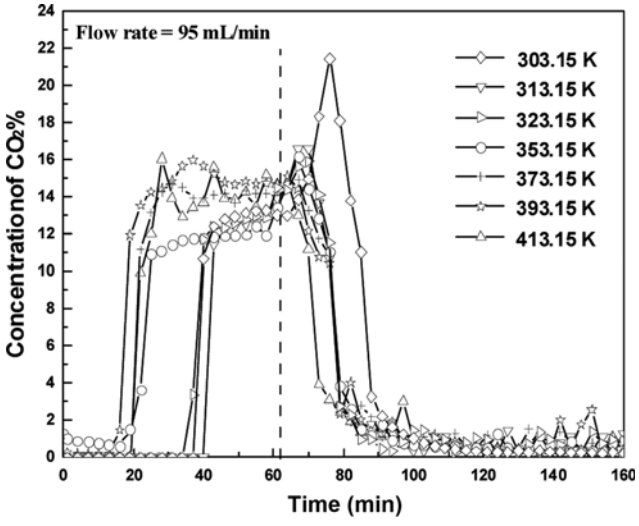

Fig. 12. Adsorption-desorption curves at different adsorption temperatures: flow rate of is 95 mL/min.

rial presented a total loss of mass 0.4119 mg (26.27%) between (303.15 and 1,273.15) K.

The first of these weight loss events obtained below 473.15 K was characteristic of sample hygroscopicity [50] (the loss of molecular water from the exchange layer "interlayer water"). The amount of water uptake of silicate material sample depends on the relative humidity of the environment to which they are exposed. Until 799.15 K, the second loss of weight occurs due to the removal of water composition from the silicate mineral [51]. The third weight loss occurring in sample corresponds to the dehydroxylation of the silicate material. This is shown as a peak centered at 1,173.15 K event in the DSC curve. The weight loss during the dehydroxylation of the silicate material was about 5.49% between (928.15 and 1,173.15) K and corresponds to decomposition of $CaCO_3$ [47].

2. Adsorption of CO_2 on Silicate Material

As the time went by, increasing amounts of CO_2 continually took up the silicate material adsorbent bed. The composition of outlet gas stream on the bed was continuously monitored. Then, a number of gases from the adsorption column were followed as the fraction of effluent gas concentrations, resulting in over the input gas concentration. So the method agrees with practical conditions, temperatures and multicomponent streams; and the dynamic adsorption capacities of the materials can be calculated.

Under equilibrium conditions, the increase/decrease of flow rate in a fixed bed at a constant temperature concentration of the adsorbable species should not affect the adsorption capacity. In this work, we first determined 15.79% (vol) CO_2 on the surface of silicate material at flow rate=95 mL/min and T=303.15 K (Fig. 11).

Fig. 11 shows the beginning breakthrough time at 13 min. The dynamic adsorption capacity was calculated at 9.34 mg/g.

Two methods, including programmed heating the packed column up to 423.15 K and reflux purging using N_2, joined to the aim of desorption. It can be seen that the captured CO_2 is quickly desorbed after the gas carrier has been switched from CO_2/N_2 mixtures to N_2. In fact, the desorbed rate of silicate material is over 90% within 12 min when the flow rate of N_2 is above 95 mL/min.

2-1. Effect of Temperature

The silicate material was subjected to adsorption performance studies at flow rates of 95 mL/min with 15.79% CO_2 (Fig. 12).

From Fig. 12, when the flow rate was 95 mL/min, the diversities of adsorption-desorption curves were obvious, which means adsorption temperature is more leading than flow rate. The curves at temperatures of 303.15, 313.15, and 323.15 K were separated from the other four desorption curves at temperatures of 353.15, 373.15, 393.15, and 413.15 K in the flow rate of 95 mL/min, which signifies the selection of above 323.15 K as the optimum adsorption temperature. The dynamic adsorption capacity decreased from 9.34 to 5.49 mg/g when the adsorption temperature was increased from 303.15 to 413.15 K.

Fig. 12 shows that silicate material is an adsorbent with wide temperature range of application. The amount of CO_2 adsorbed decreased with increasing adsorption temperatures, because CO_2 physical sorption is an exothermic process [52]. The lower adsorption temperature benefits CO_2 adsorption on the silicate material.

We calculated the thermodynamic data of our experiments. As is shown in the following, the ΔG^o can be calculated:

$$\Delta G^o = -RT \ln K_e \quad (1)$$

The K_e value was calculated using the following equation:

$$K_e = q_e/C_e \quad (2)$$

Relation among ΔG^o [53], enthalpy change (ΔH^o) [54] and entropy change (ΔS^o) [55] could be expressed by the following equation:

$$\Delta G^o = \Delta H^o - T\Delta S^o \quad (3)$$

Eq. (3) could be written as:

$$\ln K_e = -\frac{\Delta G^o}{RT} = -\frac{\Delta H^o}{RT} + \frac{\Delta S^o}{R} \quad (4)$$

According to Eq. (4), ΔH^o and ΔS^o values could be calculated from the slope and intercept of the plot of ln K_e versus 1/T, respectively.

As is shown in Table 5, the negative ΔG^o values indicated that the process was thermodynamically feasible, spontaneous and chemically controlled. The negative value of ΔH^o indicates that the adsorption process was exothermic. The negative value of ΔS^o shows the decreased randomness and reduced confusion at the solid/gas interface during the adsorption process.

We analyzed the adsorption capability of CO_2 on the HACFA was by Langmuir model equation. By fitting the adsorption isotherm, the linear form of the Langmuir isotherm equation was represented by the following equation:

$$\frac{1}{q_0} = \frac{1}{q_{max} K_L} \times \frac{1}{C_0} + \frac{1}{q_{max}} \quad (5)$$

Table 5 shows the calculated Langmuir isotherm parameter, and their corresponding coefficient of determination, R^2 values.

Table 5. ΔG^o, ΔH^o and ΔS^o data of CO_2 adsorption process

T (K)	ΔG^o (kJ/mol)	ΔH^o (kJ/mol)	ΔS^o (J/mol)
303.15	−4.52	−7.03	−16.63
313.15	−5.79	−9.24	−17.84
323.15	−5.21	−9.39	−16.92
353.15	−5.61	−9.91	−17.21
373.15	−6.06	−10.03	−19.84
393.15	−4.97	−8.89	−18.32
413.15	−5.88	−9.99	−19.13

Table 6. Langmuir isotherm data of CO_2 adsorption process

Temperature (°C)	q_{max} (mg/L)	K_L (L/mg)	R^2
30	9.34	0.349	0.9977
40	9.96	0.594	0.9977
50	9.24	0.124	0.9987
80	6.70	0.539	0.9981
100	5.40	1.038	0.9939
120	4.22	3.459	0.9900
140	5.49	2.043	0.9901

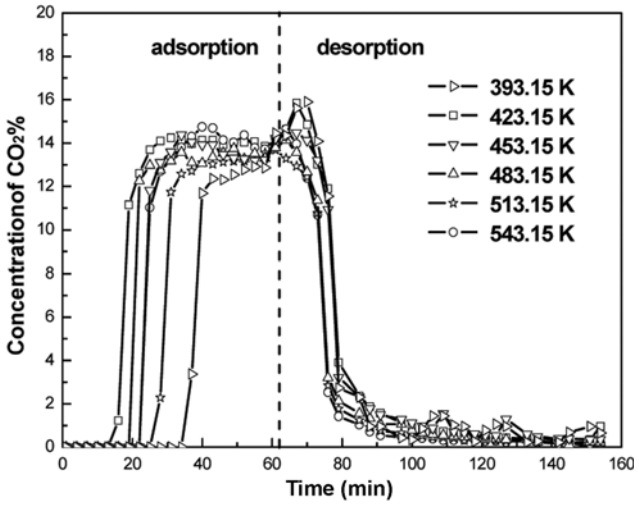

Fig. 13. Adsorption-desorption curves at different drying temperatures: flow rate is 95 mL/min and adsorption temperature is 323.15 K.

Langmuir equation fitted all the samples well with coefficients (R^2) in the range of 0.9900-0.9987 (Table 6), which was reasonably applied in all cases. This phenomenon illustrated that adsorption of CO_2 on the HACFA conformed to the Langmuir isotherm model, which assumes uniform energies of adsorption on the surface and no transmigration of adsorbents on the surface. Table 5 gives Langmuir constants for the silicate material at different temperature.

The pseudo-first and second order gas solid adsorption models are the most widely used because they are simple to describe the adsorption kinetics and the adsorbent-adsorbate interactions. In the present study, these two models were first used to describe the CO_2 adsorption behavior of the silicate material under a wide range of CO_2 partial pressure and adsorption temperature. The correlated kinetic parameters were also obtained through the fitting of adsorption model with experimental adsorption curves.

Kinetic parameters of pseudo-first order and pseudo-second order models under different adsorption conditions were at the flow rate of 95 mL/min with 15.79 % CO_2. From Table 6, the normalized standard deviation (Δq) of pseudo-second order model was smaller than that of pseudo-first order model. Therefore, the pseudo-second order model was more suitable to predict the CO_2 adsorption process of the silicate material in our experiments[56]. As mentioned above, the pseudo-second order model was suited to describe the adsorption process involving chemical adsorption [57].

2-2. Effect of Moisture

Adsorption performance of silicate material was observed when the material was dried at 393.15 K for 3 h. To see the effect of moisture, pre-drying to silicate material at different temperatures was applied. Fig. 14 was obtained with flow rate of 95 mL/min and adsorption temperature of 323.15 K. The dynamic adsorption capacity followed a flexural trend at 9.24, 4.82, 6.20, 5.76, 7.48, and 6.06 mg/g when the pre-drying temperature was increased from 393.15 to 543.15 K at a step of 30 K in Fig. 14.

CO_2 adsorption at pre-drying temperature of 393.15 K was superior to other pre-drying temperatures, which was explained by the

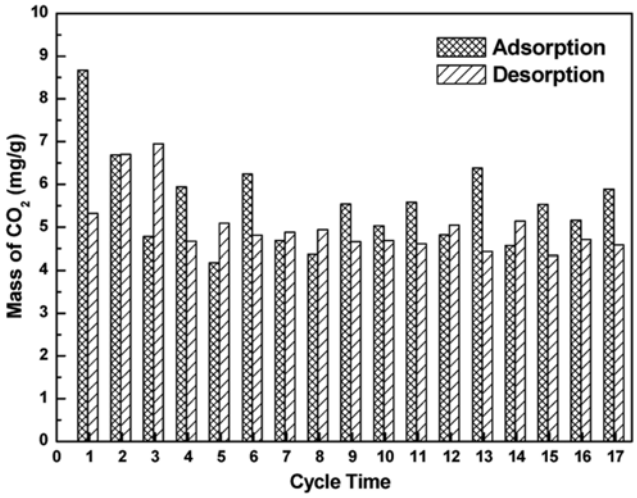

Fig. 14. Recycling data for silicate material on adsorption of CO_2. * Flow rate=95 mL/min; adsorption temperature=323.15 K.

hydration interaction of CO_2 and adsorbed water on adsorbent surface [58]. The effect of moisture was conspicuous, which reflects the positive influence of water vapor toward adsorption performance, and maybe the phenomena resulted from the mass of Si-OH on the surface of silicate material.

2-3. Regeneration of Silicate Material

Excellent regeneration is a requirement of CO_2 sorbents. The regeneration capacity of silicate material was tested by means of adsorption-desorption cycles at 323.15 K, and flow rate was 95 mL/min with 15.79% CO_2. The CO_2 adsorption -desorption results on silicate materials are presented in Fig. 14. These adsorption-desorption cycles were repeated seventeen times and no noticeable changes were observed in desorption process or CO_2 uptake. For the first time, the dynamic CO_2 adsorption of silicate material provided the maximum adsorption capacity of 8.67 mg/g, which failed to provide any further improvement at the subsequent times. The adsorption capacity remained fluctuating as the recycling time increased, and it declined marginally to 5.89 mg/g for the seventeenth time. Fig. 14 shows the differences between adsorption and desorption in every single experiment. For example, for the first time compared with the desorption capacity of 5.23 mg/g, the capacity of CO_2 adsorption is obtained to 8.67. The desorption capacity of 5.23 mg/g resulted from physical interaction on the surface of material, and the difference of 3.44 indicates the chemical reaction between alkaline silicate material and CO_2.

Thus, the reported silicate materials can be quickly, easily, and

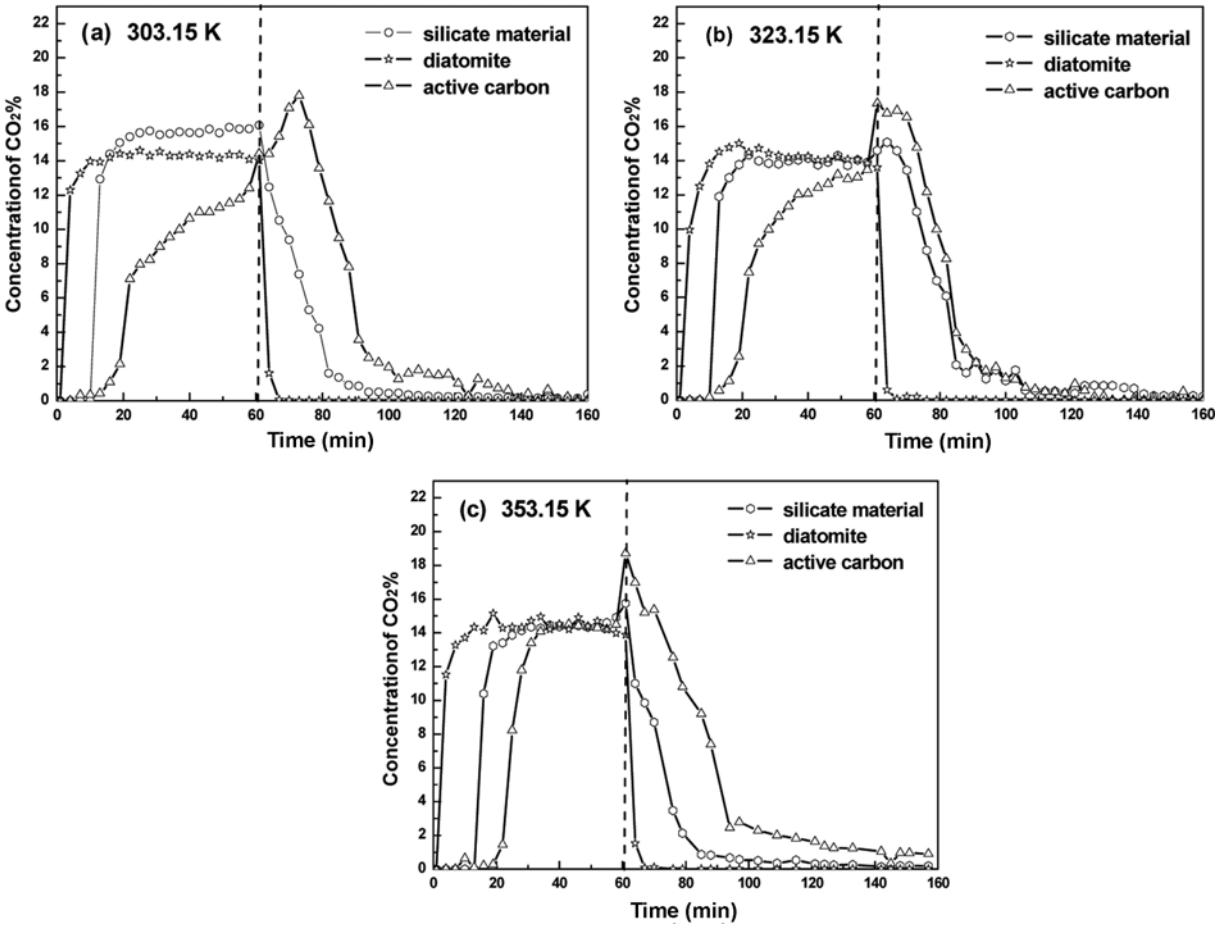

Fig. 15. Adsorption-desorption curves for three adsorbents on CO_2: flow rate is 95 mL/min, and adsorption temperature of (a) is 303.15 K, (b) is 323.15 K, and (c) is 353.15 K.

totally regenerated over multiple cycles without any loss of adsorption performance. Deeply, silicate material was a potential sorbent to CO_2 removal.

3. Adsorption Comparison of CO_2 on Various Materials

Comparative curves for CO_2 adsorption curves on silicate material, commercial active carbon, and commercial diatomite at 303.15, 323.15, and 353.15 K are presented in Fig. 15. The three adsorbents were evaluated at the flow rate of 95 mL/min with 15.79% CO_2. It is seen that the CO_2 capture capacities on the silicate materials are quite substantial (8.24 mg/g, 7.31 mg/g, and 5.08 mg/g, respectively) and more importantly, they exhibit a superior CO_2 capture capacity to that of diatomite (3.18 mg/g, 3.43 mg/g and 3.05 mg/g, respectively). The CO_2 capture capacity of commercial active carbon (14.59, 12.95 and 12.06 mg/g) is better than the other two adsorbents. The investigation of dynamic adsorption behavior shows that the silicate material presents similar adsorption properties with commercial active carbon and stronger adsorption properties than commercial diatomite.

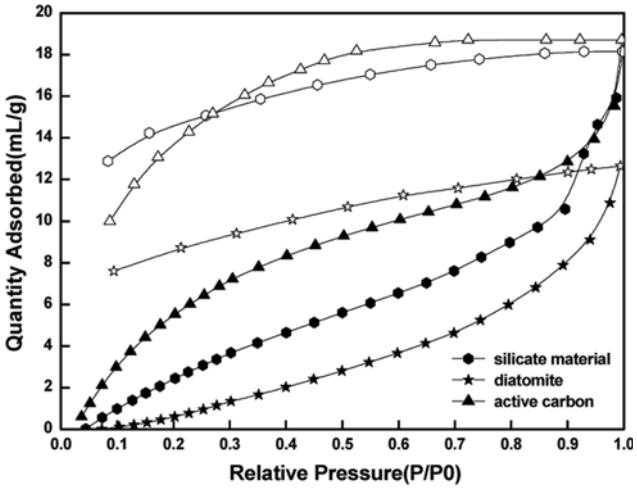

Fig. 16. Adsorption-desorption isotherms for three adsorbents on CO_2. * Solid - adsorption; hollow - desorption.

Experimental results of adsorption-desorption isotherms at 273.15 K are summarized in Fig. 16 for CO_2 capture by the specific surface and pore size analysis instrument using silicate material, diatomite and active carbon. Fig. 16 indicates the same tendency compared with Fig. 15. The CO_2 adsorption capacity of silicate material is higher than that of diatomite at the same CO_2 partial pressure, but lower than that of active carbon. Meanwhile, extreme hysteresis loops were also observed, indicating the existence of mesopores in all three adsorbents, which was confirmed by the results of nitrogen adsorption.

Table 1 and Table 3 show the differences in surface area and pore characteristic data of the three adsorbents. The specific surface area of active carbon is mainly quadruple to active carbon, and the specific pore volume of active carbon to silicate material ratio is 2 : 1. These two adsorbents have similar average pore diameter, and the experiment data of diatomite are obviously less than the data of active carbon and silicate material. These results demonstrate that the CO_2 capture capacity on the sorbents not only depends on the textural properties (i.e., BET surface area or pore volume), but also on the pore size distribution, as recent research works have shown that active carbons with a large population of pores of size 1-2 nm exhibit a better CO_2 adsorption performance than those with narrower micropores or with a mesoporous pore network [59-61].

Also, although the silicate material displays less capture capacity than commercial active carbon, it has a considerably lower price and higher potential to protect the environment.

In summary, the main pore distribution between 3 and 20 nm and small pore system with micropore (1.5-2.0 nm) of silicate material provides the adsorptive sites on CO_2. Some adsorbed water and/or crystal water existed to react with CO_2. Alkaline silicate

Table 7. Pseudo-first and second order data of CO_2 adsorption process

T (°C)	q_e (mg/g)	Pseudo-first order			Pseudo-second order		
		q_c (mg/g)	k_f	Error Δq (%)	q_c (mg/g)	k_s	Error Δq (%)
30	13.25	13.16	0.176	0.68	13.22	0.136	0.23
40	12.96	11.82	0.088	8.80	12.54	0.042	3.24
50	12.91	12.53	0.029	2.94	12.77	0.136	1.08
80	12.40	12.13	0.021	2.18	12.30	0.180	0.81
100	14.66	13.36	0.089	8.87	14.18	0.035	3.27
120	15.94	12.90	0.056	19.07	15.61	0.074	2.07
140	16.04	13.64	0.150	14.96	15.57	0.048	2.93

Table 8. Thomas model parameters at different original concentrations, flow rates

V (mg/L)	C_0 (mL/min)	x (g)	K_{th} (10^{-3} L/(min·mg))	q_0 (mg/g)	R^2
95	13.25	130	8.378	7.501	0.9910
190	15.86	130	8.453	5.990	0.9902
285	15.38	130	4.556	4.407	0.9924
380	15.35	130	6.065	7.577	0.9906
475	15.68	130	4.238	6.321	0.9913

material is a good adsorbent for the acidic gas CO_2, and the experiment of modified silicate material is in expectation to further improve the performance of CO_2.

3. Thomas Model

We also studied our experimental results by the Thomas model. Thomas model parameters at different original concentrations, flow rates are shown in Table 8. The Thomas model was suitable to predict the CO_2 adsorption process of the HACFA in our experiments. It can also describe the dynamic characteristics of CO_2 adsorption on HACFA, and can be used to predict the straw of the dynamic adsorption of CO_2 adsorption column.

CONCLUSION

The amorphous silicate material from high-alumina fly ash is composed of O, C, Si, Ca, Na, Mg, Al, and Fe, which exist as the formations of Ca^{2+}, Na^{2+}, Mg^{2+}, Al^{3+}, Fe^{3+}, SiO_3^{2-}, and CO_3^{2-}. Some adsorbed water and/or crystal water existed in the silicate material. When the material was used to impart interaction sites for CO_2 adsorption, a dynamic adsorption capacity of the silicate material for CO_2 of 8.67 mg/g at 323.15 K and flow rate=95 mL/min with 15.79% CO_2 was found based on dynamic adsorption method. The silicate material was significantly excellent to adsorb CO_2 at wide temperatures (293.15 to 413.15) K, and the adsorption ability decreased weakly with seventeen recycling times. The investigation of dynamic adsorption behavior shows that the silicate material presents adsorption properties similar to commercial active carbon and stronger adsorption properties than commercial diatomite.

The thermodynamic data of our experiments were calculated. The negative ΔG^o values indicated that the process was thermodynamically feasible, spontaneous and chemically controlled. The negative value of ΔH^o indicated that the adsorption process was exothermic. The negative value of ΔS^o showed the decreased randomness and reduced confusion at the solid/gas interface during the adsorption process. Langmuir equation fitted result illustrated adsorption of CO_2 on the HACFA assuming uniform energies of adsorption on the surface and no transmigration of adsorbents on the surface. Kinetic parameters of pseudo-first order and pseudo-second order models under different adsorption conditions were studied. Thomas model parameters at different original concentrations: Therefore, the Thomas model was suitable to predict the CO_2 adsorption process of the HACFA in our experiments. This model can also describe the dynamic characteristics of CO_2 adsorption on HACFA, and can be used to predict the straw of the dynamic adsorption of CO_2 adsorption column.

ACKNOWLEDGEMENTS

This work was supported by the Program for New Century Excellent Talents in University (NCET-12-1017), National Natural Science Foundation of China (21466028), the Program for Grassland Excellent Talents of Inner Mongolia Autonomous Region, Program for Young Talents of Science and Technology in Universities of Inner Mongolia Autonomous Region, the Research Fund for the Doctoral Program of Higher Education of China (20111514120002), the Inner Mongolia Science and Technology Key Projects, training plan of academic backbone in youth of Inner Mongolia University of Technology, and School Scientific Research Fund (X201306, Inner Mongolia University of Technology).

REFERENCES

1. D. J. Hofmann, J. H. Butler and P. P. Tans, *Atmos. Environ.*, **43**, 2084 (2009).
2. J. C. M. Pires, F. G. Martins, M. C. M. Alvim-Ferraz and M. Simões, *Chem. Eng. Res. Des.*, **89**, 1446 (2011).
3. H. Li, J. P. Jakobsen, Ø. Wilhelmsen and J. Yan, *Appl. Energy*, **88**, 3567 (2011).
4. A. Nuchitprasittichai and S. Cremaschi, *Int. J. Greenh. Gas Con.*, **13**, 34 (2013).
5. N. Hiyoshi, K. Yogo and T. Yashima, *Micropor. Mesopor. Mater.*, **84**, 357 (2005).
6. L. S. Tan, A. M. Shariff, K. K. Lau and M. A. Bustam, *J. Ind. Eng. Chem.*, **18**, 1874 (2012).
7. J. K. Adewole, A. L. Ahmad, S. Ismail and C. P. Leo, *Int. J. Greenh. Gas Con.*, **17**, 46 (2013).
8. D. Berstad, R. Anantharaman and P. Neksa, *Int. J. Refrig.*, **36**, 1403 (2013).
9. J. N. Knudsen, J. N. Jensen, P. J. Vilhelmsen and O. Biede, *Energy Procedia*, **1**, 783 (2009).
10. R. Bounaceur, N. Lape, D. Roizard, C. Vallieres and E. Favre, *Energy*, **31**, 2556 (2006).
11. A. Hart and N. Gnanendran, *Energy Procedia*, **1**, 697 (2009).
12. B. ZareNezhad and N. Hosseinpour, *Energy Convers. Manage.*, **50**, 1491 (2009).
13. V. P. Mulgundmath, R. A. Jones, F. H. Tezel and J. Thibault, *Sep. Pur. Technol.*, **85**, 17 (2012).
14. S. Himeno, T. Komatsu and S. Fujita, *J. Chem. Eng. Data*, **50**, 369 (2005).
15. A. A. Olajire, *Energy*, **35**, 2610 (2010).
16. M. G. Plaza, C. Pevida, B. Arias, J. Fermoso, M. D. Casal and C. F. Martín, *Fuel*, **88**, 2442 (2009).
17. N. A. Rashidi, S. Yusup and B. H. Hameed, *Energy*, **61**, 440 (2013).
18. R. V. Siriwardane, M. S. Shen and E. P. Fisher, *Energy Fuel*, **19**, 1153 (2005).
19. I. Majchrzak-Kuceba and W. Nowak, *Thermochim. Acta*, **437**, 67 (2005).
20. C. Stewart and M. Hessami, *Energy Convers. Manage.*, **46**, 403 (2005).
21. Z. T. Yao, M. S. Xia, P. K. Sarker and T. Chen, *Fuel*, **120**, 74 (2014).
22. M. Ilic, C. Cheeseman, C. Sollars and J. Knight, *Fuel*, **82**, 331 (2003).
23. V. Manoharan, I. A. M. Yunusa, P. Loganathan, R. Lawrie, C. G. Skilbeck and M. D. Burchett, *Fuel*, **89**, 3498 (2010).
24. H. Lee, H. S. Ha, C. H. Lee, Y. B. Lee and P. J. Kim, *Bioresour. Technol.*, **97**, 1490 (2006).
25. M. Erol, S. Kucukbayrak and A. Ersoy-Mericboyu, *Fuel*, **87**, 1334 (2008).
26. M. Erol, S. Kucukbayrak and A. Ersoy-Mericboyu, *J. Hazard. Mater.*, **153**, 418 (2008).
27. J. Fang, G. Qin, W. Wei and X. Zhao, *Sep. Pur. Technol.*, **80**, 585 (2011).

28. D. Jain, C. Khatri and A. Rani, *Fuel Process. Technol.*, **91**, 1015 (2010).
29. E. Saputra, S. Muhammad, H. Q. Sun, H. M. Anga, M. O. Tadéa and S. B. Wang, *Catal Today*, **190**, 68 (2012).
30. X. P. Xuan, C. T. Yue, S. Y. Li and Q. Yao, *Fuel*, **82**, 575 (2003).
31. S. B. Wang and H. W. Wu, *J. Hazard Mater.*, **136**, 482 (2006).
32. Y. Li, F. Zhang and F. Xiu, *Sci. Tot. Environ.*, **407**, 5780 (2009).
33. M. Niewiadomski, J. Hupka, R. Bokotko and J. D. Miller, *Fuel*, **78**, 161 (1999).
34. M. Chareonpanich, T. Namto, P. Kongkachuichay and J. Limtrakul, *Fuel Process. Technol.*, **85**, 1623 (2004).
35. Z. T. Yao, Y. Ye and M. S. Xia, *Environ. Prog. Sustain.*, **32**, 790 (2013).
36. D. Wu, B. Zhang, L. Yan, H. Kong and X. Wang, *Int. J. Miner. Process.*, **80**, 266 (2006).
37. A. Hernandez-Exposito, J. M. Chimenos, A. I. Fernandez, O. Font, X. Querol, P. Coca and F. Garcia Pena, *Chem. Eng. J.*, **118**, 69 (2006).
38. F. Arroyo Torralvo and C. Fernández-Pereira, *Miner. Eng.*, **24**, 35 (2011).
39. A. Shemi, R. N. Mpana, S. Ndlovu, L. D. van Dyk, V. Sibanda and L. Seepe, *Miner. Eng.*, **34**, 30 (2012).
40. S. Dinda, *Sep. Pur. Technol.*, **109**, 64 (2013).
41. J. M. Sun, Z. J. Zhang, G. Chen, S. Y. Yan, Q. Z. Huo and L. C. Wu, The method of active calcium silicate in the produce process of Al_2O_3 using high-alumina fly ash. CN. Patent. CN102249253A (2011).
42. Z. J. Zhang, J. M. Sun, H. F. Cao, X. Y. Zhang, Y. W. Wang and Q. Yao, A synthetical method of calcium silicate powder using high-alumina fly ash. CN. Patent. CN101591023 (2008).
43. R. R. Yadav, S. N. Mudliarb, A. Y. Shekh, A. B. Fulke, S. S. Devi, K. Krishnamurthi, A. Juwarkar and T. Chakrabarti, *Process Biochem.*, **47**, 585 (2012).
44. Y. Mogami, S. Yamazaki, S. Matsuno, K. Matsui, Y. Noda and K. Takegoshi, *Cement Concrete Res.*, **66**, 115 (2014).
45. Y. Q. Zhang, A. V. Radha and A. Navrotsky, *Geochim. Cosmochim. Ac.*, **115**, 92 (2013).
46. P. Tien and L. K. Chau, *Chem. Mat.*, **11**, 2141 (1999).
47. H. Zaitan, D. Bianchi, O. Achak and T. Chafik, *J. Hazard. Mater.*, **153**, 852 (2008).
48. R. A. Nyquist, C. L. Putzig and R. O. Kagel, Anne Leugers M. Infrared spectra of inorganic compounds. Michigan: Academic Press (1971).
49. T. Tsoncheva, G. Issa, T. Blasco, M. Dimitrov, M. Popova and S. Hernadez, *Appl. Catal. A: Gen.*, **453**, 1 (2013).
50. M. V. Kok, *Energy Sources*, **24**, 907 (2005).
51. F. Ayari, E. Srasra and M. Trabelsi-Ayadi, *Desalination*, **185**, 391 (2005).
52. M. Sevilla and A. B. Fuertes, *J. Colloid Interface Sci.*, **366**, 147 (2012).
53. H. Ucun, Y. K. Bayhan and Y. Kaya, *J. Hazard. Mater.*, **153**, 52 (2008).
54. T. Fan, Y. Liu, B. Feng, G. Zeng, C. Yang, M. Zhou, H. Zhou, Z. Tan and X. Wang, *J. Hazard. Mater.*, **160**, 655 (2008).
55. S. M. Tuzen, O. D. Uluözlü and M. Soylak, *Biochem. Chem. Eng. J.*, **37**, 151 (2007).
56. J. M. Borah, J. Sarma and S. Mahiuddin, *Colloids Surf., A*, **387**, 50 (2011).
57. R. Serna-Guerrero and A. Sayari, *Chem. Eng. J.*, **161**, 182 (2010).
58. J. Baltrusaitis and V. H. Grassian, *J. Phys. Chem. B*, **109**, 12227 (2005).
59. A. Wahby, J. M. Ramos-Fernandez, M. Martinez-Escandell, A. Sepulveda-Escribano, J. Silvestre-Albero and F. Rodriguez-Reinoso, *ChemSusChem*, **3**, 974 (2010).
60. M. Sevilla, P. Valle-Vigón and A. B. Fuertes, *Adv. Funct. Mater.*, **21**, 2781 (2011).
61. M. Sevilla and A. B. Fuertes, *Energy Environ. Sci.*, **4**, 1765 (2011).